

The Optical Gravitational Lensing Experiment. Ellipsoidal Variability of Red Giants in the Large Magellanic Cloud*

I. Soszyński^{1,2}, A. Udalski¹, M. Kubiak¹,
M.K. Szymański¹, G. Pietrzyński^{1,2}, K. Żebruń¹,
O. Szewczyk¹, Ł. Wyrzykowski¹
and W.A. Dziembowski¹

¹Warsaw University Observatory, Al. Ujazdowskie 4, 00-478 Warszawa, Poland
e-mail:

(soszynsk,udalski,mk,msz,pietrzyn,zebrun,szewczyk,wyrzykow,wd)@astrouw.edu.pl

² Universidad de Concepción, Departamento de Física, Casilla 160-C, Concepción,
Chile

ABSTRACT

We used the OGLE-II and OGLE-III photometry of red giants in the Large Magellanic Cloud to select and study objects revealing ellipsoidal variability. We detected 1546 candidates for long period ellipsoidal variables and 121 eclipsing binary systems with clear ellipsoidal modulation. The ellipsoidal red giants follow a period–luminosity (PL) relationship (sequence E), and the scatter of the relation is correlated with the amplitude of variability: the larger the amplitude, the smaller the scatter.

We note that some of the ellipsoidal candidates exhibit simultaneously OGLE Small Amplitude Red Giants pulsations. Thus, in some cases the Long Secondary Period (LSP) phenomenon can be explained by the ellipsoidal modulation.

We also select about 1600 red giants with distinct LSP, which are not ellipsoidal variables. We discover that besides the sequence D in the PL diagram known before, the LSP giants form additional less numerous sequence for longer periods. We notice that the PL sequence of the ellipsoidal candidates is a direct continuation of the LSP sequence toward fainter stars, what might suggest that the LSP phenomenon is related to binarity but there are strong arguments against such a possibility.

About 10% of the presented light curves reveal clear deformation by the eccentricity of the system orbits. The largest estimated eccentricity in our sample is about 0.4.

All presented data, including individual BVI observations and finding charts are available from the OGLE Internet archive.

binaries: close – binaries: eclipsing – Stars: late-type – Magellanic Clouds

*Based on observations obtained with the 1.3 m Warsaw telescope at the Las Campanas Observatory of the Carnegie Institution of Washington.

1. Introduction

Ellipsoidal variability is a phenomenon often observed in close binary systems. It is caused by aspect changes of the component deviated from spherical symmetry by tidal interactions with its companion. A typical ellipsoidal light curve is sinusoidal-shaped, with two maxima and two minima per orbital period. Light variations should peak at orbital phases 0.25 and 0.75, when maximal area of the Roche-lobe is projected. In general the depths of the minima are not equal, which is the result of next order effects of the tidal distortion.

Ellipsoidal variables are relatively rarely studied objects, and long period ellipsoidal variables are almost unknown. Morris (1985) gathered all ellipsoidal variables known at that time, and listed 20 confirmed and 20 suspected objects of this type. Only one variable star from this catalog (T CrB) had period longer than 100 days. Since then, the number of known ellipsoidal variables has increased, but still, the list of confirmed ellipsoidal red giants is very short. However, the analysis of the ellipsoidal variations is a useful tool for studying various types of close binary systems: X-ray binaries, cataclysmic binaries, symbiotic stars, early type near contact systems.

In recent years gravitational microlensing surveys have revolutionized our knowledge about variable red giants. Wood *et al.* (1999) presented period–luminosity (*PL*) diagram of the long period variables which showed series of distinct parallel sequences, marked with letters A–E.

In the previous paper (Soszyński *et al.* 2004), we selected and studied about 15 000 red giants occupying most often the sequence A. We showed that these objects, named by Wray, Eyer and Paczyński (2004) OGLE Small Amplitude Red Giants (OSARG), constitute a separate type of pulsating giants, different than “classical” semi-regular variables (SRV).

In this paper we present a sample of variable red giants constituting *PL* sequence E, spreading below the sequences A–D. Wood *et al.* (1999) suggested that most of these stars are contact binaries. We studied photometry of these objects and noticed that, indeed, the majority of the light curves are probably ellipsoidal or eclipsing close binary systems. Our sample is, then, a natural extension of the catalog of eclipsing binary systems in the LMC prepared by Wyrzykowski *et al.* (2003).

2. Observations and Data Reductions

Observations presented in this paper were carried out with the 1.3-m Warsaw telescope at the Las Campanas Observatory, Chile, operated by the Carnegie Institution of Washington. Central parts of the LMC were added to the list of regularly monitored fields in January 1997, *i.e.*, at the beginning of the second phase of the OGLE project (OGLE-II). The telescope was then equipped with the “first generation” camera with the SITe 2048 × 2048 CCD detector. The pixel size was 24 μm resulting in 0.417 arcsec/pixel scale. Observations of the LMC were performed in the “slow” reading mode of the CCD detector

with the gain $3.8 e^-/\text{ADU}$ and readout noise of about $5.4 e^-$. Details of the instrumentation setup can be found in Udalski, Kubiak and Szymański (1997).

In June 2001 the third stage of the OGLE experiment (OGLE-III) began. The Warsaw telescope was equipped with a “second generation” CCD mosaic camera consisting of eight SITe ST-002a CCD detectors with 2048×4096 pixels of $15 \mu\text{m}$ size (Udalski 2003). This corresponds to $0.26 \text{ arcsec/pixel}$ scale and the field of view of the whole mosaic $35' \times 35'$. The last observations presented in this paper were collected in May 2004.

The vast majority of the observing points (430–860, depending on the field) were obtained through the I filter, while in the V and B -bands several dozen measurements were collected. The OGLE BVI filters closely resemble the standard system. OGLE-II I -band photometry was obtained using the Difference Image Analysis (DIA) method – image subtraction algorithm developed by Alard and Lupton (1998) and Alard (2000), and implemented by Woźniak (2000). OGLE-III magnitudes come from the standard data pipeline (Udalski 2003). V and B -band photometry was performed with the modified version of the DOPHOT package (Schechter, Mateo and Saha 1993). OGLE-II and OGLE-III data were tied in the identical manner as in Soszyński *et al.* (2004).

3. Selection of the Ellipsoidal Candidates

We performed the period analysis for every star brighter than $I = 18 \text{ mag}$. We used I -band light curves, for which the majority of observations had been collected and ran FNPEAKS program (Kołaczkowski 2003, private communication) to derive the most significant periodicities.

For further analysis we selected stars with significant periodic light variations, *i.e.*, objects for which the ratio of the highest peak in the periodogram to the mean value was higher than 8. For this sample we constructed the $\log P - W_I$ diagram, where W_I is reddening free Wesenheit index, defined as:

$$W_I = I - 1.55(V - I)$$

where I and V are intensity mean magnitudes and 1.55 is the mean ratio of total-to-selective absorption ($A_I/E(V - I)$). It appears that $\log P - W_I$ diagrams can successfully replace period – near-infrared magnitude diagram, commonly used in the variable red giants studies.

Our $\log P - W_I$ diagram shows a series of sequences, presented for the first time by Wood *et al.* (1999), and marked by letters A–E. In this paper we analyze the sequence E, spreading below the ridges of OSARGs, SRV, Miras and Long Secondary Periods (LSP), and extending down to our limiting luminosity (18 mag).

We selected and visually inspected the light curves of stars forming the sequence E. It appears that most of these objects are characterized by nearly sinusoidal light curves with an amplitude between a few hundredths and a few tenths of magnitude. Fig. 1 presents exemplary light curves of these objects. It also appears that the majority of the light curves shows alternately shallower and

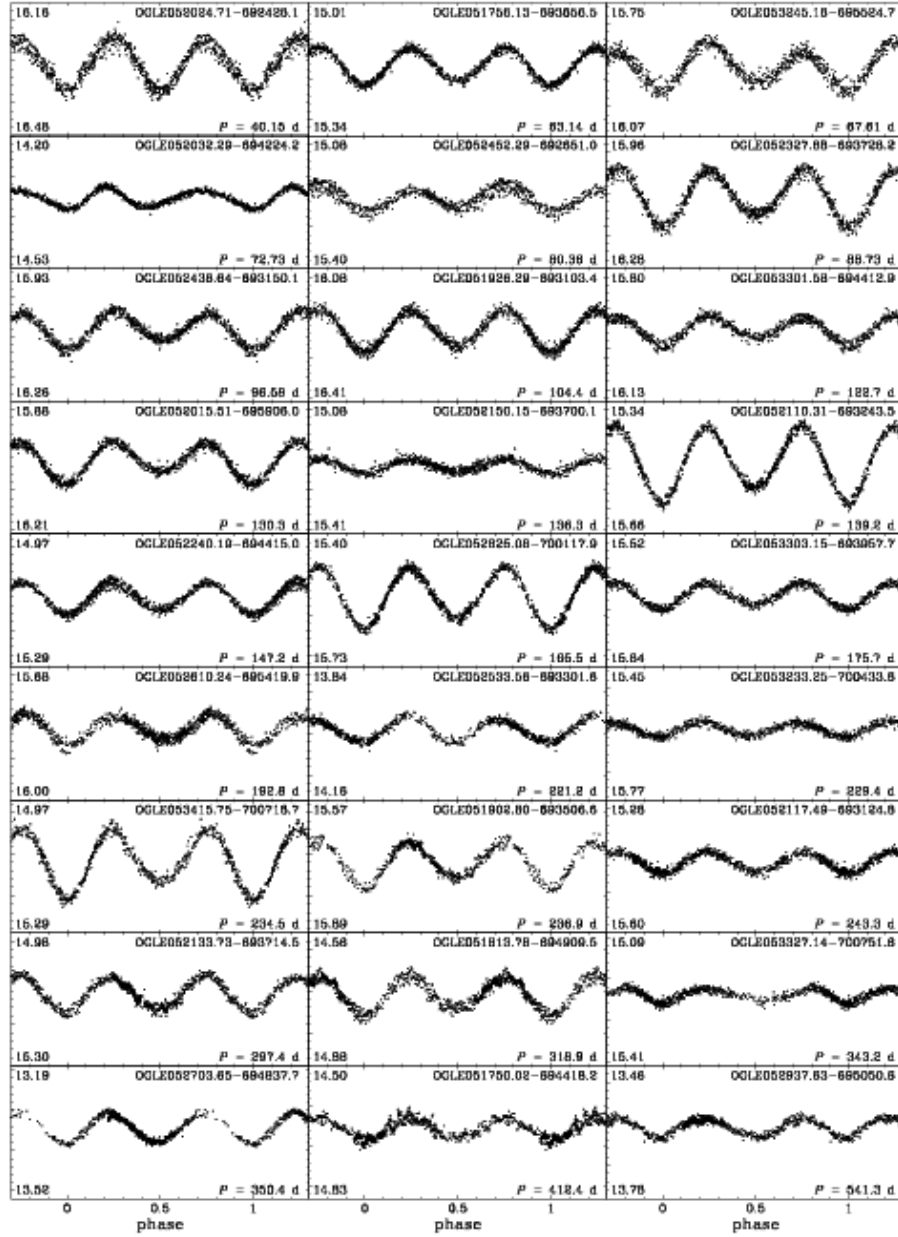


Fig. 1. Light curves of the exemplary ellipsoidal red giants in the LMC.

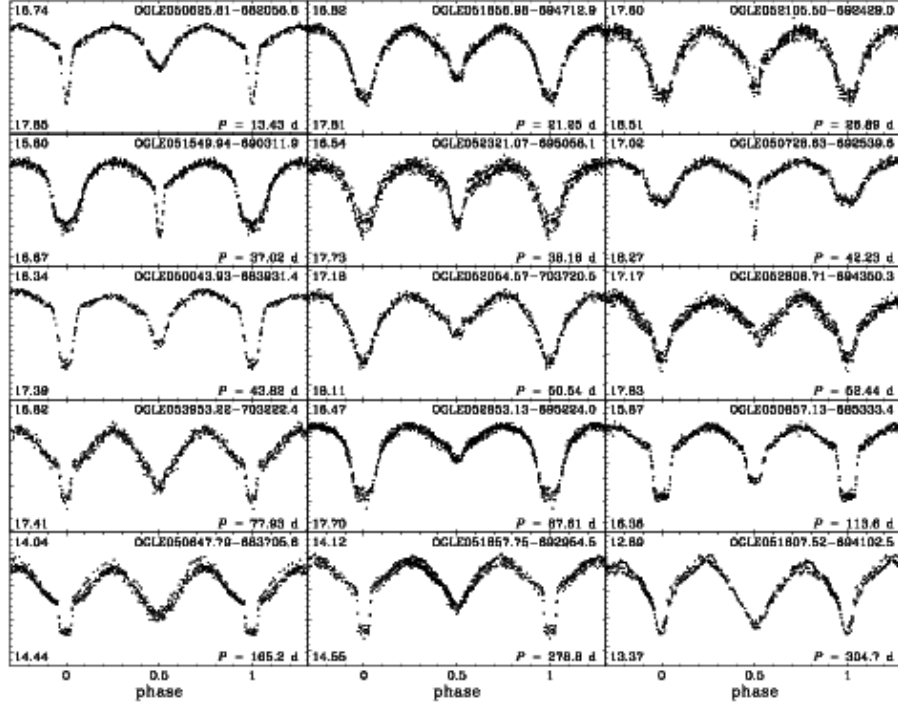


Fig. 2. Light curves of the exemplary eclipsing red giants in the LMC.

deeper minima, so the formal period is two times longer than the one obtained automatically in our period search.

Among selected objects we also found 121 eclipsing variables, most often showing clear ellipsoidal effect. Several typical light curves showing eclipses are presented in Fig. 2. We compared the eclipsing binaries with the sample of sinusoidal variables, and found that when neglecting eclipses, the shapes of the light curves from both samples are very similar.

Taking into account this similarity of the eclipsing and “sinusoidal” light curves, as well as the same position in the color–luminosity and period–luminosity diagrams, we interpret the “sinusoidal” objects as binary systems with orbital inclinations too small to cause the eclipses. Apparent variability of these objects is caused by the ellipsoidal distortion of red giants.

To confirm whether a star is or is not an ellipsoidal variable, one needs to obtain a radial velocity curve. We believe that the variability of the vast majority of selected stars are caused by ellipsoidal modulation, but one should remember that our sample may also contain a number of other types of variables. We expect such contamination especially among stars with the smallest amplitudes.

It is worth mentioning that ellipsoidal light curves which, on first sight, do not show eclipses, can actually be eclipsing variables. First, there might

be grazing eclipses, which are not detectable by visual inspection. Second, even complete eclipses can be very shallow when the radius of the secondary component is significantly smaller than the radius of the red giant. Some of these objects can be X-ray eclipsing systems, which do not show eclipses in visual pass-bands, but they are observable in X-rays.

4. Ellipsoidal and Eclipsing Variables

We selected 1546 candidates for the ellipsoidal and 121 eclipsing variables in the LMC, with periods ranging from 15 to 600 days. Table 1 lists first 70 candidates for the ellipsoidal variables from the field LMC_SC1. The following columns present star ID, star number (consistent with the LMC photometric maps, Udalski *et al.* 2000), equatorial coordinates, RA and DEC, for the epoch 2000.0, periods in days (referred to the double-peak light curves), moment of the zero phase (corresponding to the deeper minimum), intensity mean *IVB* magnitudes, larger and smaller amplitudes of the *I*-band variability and remarks.

The list of all variables is available in the electronic form from the OGLE INTERNET archive:

<http://ogle.astrouw.edu.pl/>
ftp://ftp.astrouw.edu.pl/ogle/ogle2/var_stars/lmc/ell/

or its US mirror

<http://bulge.princeton.edu/~ogle/>
ftp://bulge.princeton.edu/ogle/ogle2/var_stars/lmc/ell/

Individual *BVI* measurements of all objects and finding charts are also available from the OGLE INTERNET archive. The lists contain together 1753 entries but only 1667 objects, because 86 stars were detected twice – in the overlapping regions of adjacent fields. We decided not to remove twice-detected stars from the final list, because their measurements are independent in both fields and can be used for testing quality of the data and the completeness of the sample.

In Fig. 3 we plotted the $\log P$ – W_I diagrams for the ellipsoidal binaries. The upper panel shows variables with the largest amplitudes ($\Delta I > 0.08$ mag), the middle panel presents variables with intermediate amplitudes ($0.04 < \Delta I < 0.08$ mag), while the lower panel – stars with the smallest amplitudes ($\Delta I < 0.04$ mag). The dashed lines show the theoretical *PL* relations obtained assuming that the red giants fill up the Roche lobe. The mass of the red giant and mass of the companion were both set equal to $1M_{\odot}$. In our calculations we used Paczyński’s (1971) relation between the mean radius of the Roche lobe and the separation between components, which with the use of the Kepler law, leads to the following relation between the orbital period and mean density of the Roche lobe filling primary

$$P_{\text{orb}} = 0.12 \sqrt{\frac{\bar{\rho}_{\odot}}{\bar{\rho}}} f(q) \quad [\text{days}] \quad (1)$$

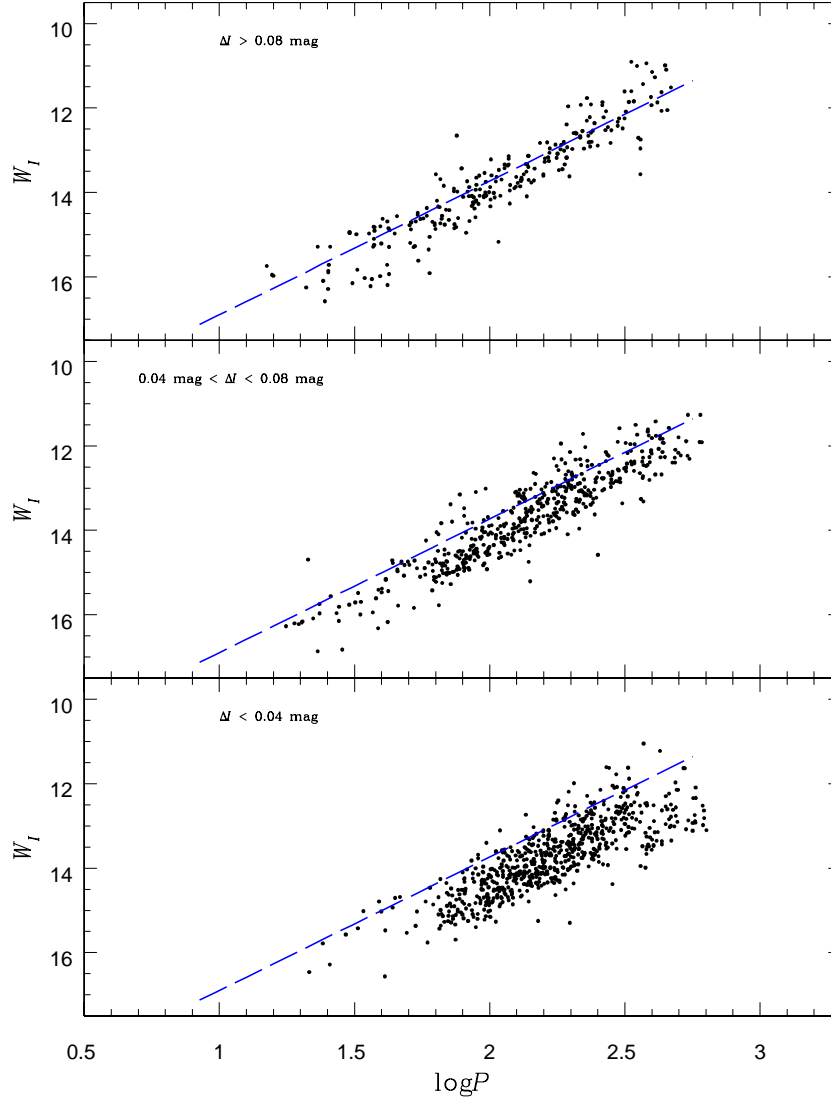


Fig. 3. Period- W_I diagrams for giants classified as ellipsoidal variables. *Upper panel* shows variables with the largest amplitudes ($\Delta I > 0.08$ mag), *middle panel* presents variables with intermediate amplitudes ($0.04 < \Delta I < 0.08$ mag), while *lower panel* stars with the smallest amplitudes ($\Delta I < 0.04$ mag).

where

$$f(q) \equiv \sqrt{(1+q)(0.38 - 0.2 \log q)^3}$$

and q is the secondary to primary mass ratio. The $f(q)$ dependence is weak: $f=3$ and 2.1 at $q=1$ and 0.1 , respectively. The values of W_I were calculated from Girardi *et al.* (2002) evolutionary tracks for the red giants phase at the

LMC composition ($X = 0.74$, $Z = 0.008$). We used Kurucz (1998) stellar atmosphere models to convert the evolutionary model parameters to the W_I values.

It is clearly seen that dispersion of the sequence E depends on the amplitude of variability. The amplitude of ellipsoidal variation is a function of the third power of the Roche-lobe filling factor (Hall 1990), therefore the variables with the largest amplitudes should be close to the limiting lines. Periods of variables with smaller amplitudes of ellipsoidal modulation may significantly depart from the theoretical limits, because giants do not entirely fill the Roche lobe.

The dispersion of data seen in the $\log P$ – W_I diagrams may be caused in part by the spread in the red giant masses. For instance, the models with $M = 1.5 M_\odot$ have the W_I values brighter by some 0.3 mag than the models with $M = 1 M_\odot$ of the same P_{orb} . Another contribution to the dispersion may arise from the the expected spread in the secondary mass, through the $f(q)$ factor in Eq. (1).

Different depths of minima, shown by the vast majority of our ellipsoidal candidates, can be explained by higher order effects of the tidal distortion. In addition, there is a number of variables in which different height of the light curve maxima is visible. This, so called O’Connell effect (Davidge and Milone 1984), is usually explained as a result of spots in the stellar surface. In some cases maximum luminosity of these objects clearly changes with time, which is probably caused by the star-spot changes. Some unequal maxima may be a result of eccentric orbit of the system (see Section 6).

5. Ellipsoidal Variability and Long Secondary Periods

Long Secondary Period (LSP) is one of the last unexplained types of stellar variability. At least 30% of the variable red giants show periods which are an order of magnitude longer than typical pulsation period of a semi-regular variable. Wood *et al.* (1999) noticed that the LSPs form a separate sequence in the period–luminosity space (sequence “D”).

Many hypotheses have been proposed to explain the LSP. Radial and non-radial pulsation, periodic dust ejection, rotation of the spotted star and binarity have been suggested as the origin of the LSPs. Recently Wood, Olivier and Kawaler (2004) ruled out most of these propositions. They argued that the most likely explanation of the LSP is a low degree g^+ mode of pulsation trapped in the outer layers above the convective envelope.

We selected from OGLE database giants with dominant period corresponding to the LSP, and then we visually inspected their light curves. We removed from the list all uncertain and doubtful variables, and left about 1600 stars in which amplitudes of the LSP are significantly larger than amplitudes of other variations. Several typical light curves folded with the long periods are shown in Fig. 4.

The period– W_I diagram for the dominant periods of these objects is shown in Fig. 5. Selected LSPs are marked with the empty circles, the magenta crosses

Table 1

Candidates for ellipsoidal variables from the field LMC_SC1 (first 70 objects)

Star ID	Star No.	RA [J2000]	DEC [J2000]	P [days]	T_0 [HJD]	I [mag]	V [mag]	B [mag]	ΔI_1 [mag]	ΔI_2 [mag]	Remarks
OGLE053404.71-703351.1	184022	5:34:04.71	-70:33:51.1	401.2	2450241.1	15.050	16.751	-	0.049	0.035	E
OGLE053450.55-703332.7	266566	5:34:50.55	-70:33:32.7	203.5	2450397.8	15.873	17.362	18.802	0.041	0.040	
OGLE053359.09-703214.4	184031	5:33:59.09	-70:32:14.4	237.9	2450353.7	15.332	17.021	18.586	0.038	0.027	
OGLE053308.28-703134.8	94879	5:33:08.28	-70:31:34.8	276.6	2450318.2	15.588	17.182	19.674	0.026	0.022	
OGLE053441.00-703117.0	266590	5:34:41.00	-70:31:17.0	286.5	2450305.1	15.449	17.107	-	0.042	0.031	
OGLE053453.25-703114.8	266550	5:34:53.25	-70:31:14.8	395.7	2450153.5	14.906	16.716	18.280	0.063	0.054	LMC_SC16
OGLE053337.07-703111.7	94832	5:33:37.07	-70:31:11.7	315.5	2450366.2	14.740	16.761	18.479	0.121	0.094	
OGLE053446.60-703005.2	271034	5:34:46.60	-70:30:05.2	275.9	2450291.0	15.981	17.428	18.814	0.026	0.017	E
OGLE053358.74-702945.1	187738	5:33:58.74	-70:29:45.1	147.8	2450420.4	16.044	17.277	18.371	0.019	0.015	
OGLE053434.16-702909.1	271103	5:34:34.16	-70:29:09.1	108.2	2450402.3	16.467	17.763	18.988	0.027	0.025	
OGLE053241.45-702908.5	4310	5:32:41.45	-70:29:08.5	225.7	2450315.7	15.655	17.268	18.860	0.040	0.028	U
OGLE053419.84-702904.2	187743	5:34:19.84	-70:29:04.2	185.7	2450446.1	15.778	17.281	18.737	0.085	0.075	
OGLE053244.29-702710.7	9238	5:32:44.29	-70:27:10.7	107.1	2450383.8	16.228	17.355	18.341	0.023	0.020	
OGLE053500.22-702643.4	275298	5:35:00.22	-70:26:43.4	286.5	2450233.4	15.215	16.705	18.138	0.035	0.016	U
OGLE053421.62-702640.5	191935	5:34:21.62	-70:26:40.5	396.6	2450353.3	14.739	16.550	18.275	0.095	0.068	
OGLE053347.67-702551.4	103381	5:33:47.67	-70:25:51.4	194.6	2450275.2	15.860	17.028	18.091	0.025	0.019	
OGLE053422.60-702355.3	192008	5:34:22.60	-70:23:55.3	165.9	2450408.8	15.983	17.384	19.666	0.052	0.045	
OGLE053401.95-702149.7	196753	5:34:01.95	-70:21:49.7	309.7	2450192.5	16.086	17.711	19.278	0.051	0.033	E
OGLE053233.48-702148.3	280177	5:34:52.53	-70:21:48.3	79.09	2450407.5	16.720	17.963	19.171	0.025	0.021	
OGLE053505.76-702135.0	280041	5:35:05.76	-70:21:35.0	274.5	2450411.5	15.227	16.915	20.484	0.040	0.031	LMC_SC16
OGLE053443.62-702116.1	280043	5:34:43.62	-70:21:16.1	476.4	2450445.1	14.793	16.196	17.404	0.200	0.107	
OGLE053349.45-701921.5	201766	5:33:49.45	-70:19:21.5	116.7	2450373.7	16.687	17.978	19.190	0.028	0.024	
OGLE053356.79-701919.6	201696	5:33:56.79	-70:19:19.6	205.6	2450306.5	16.305	17.689	18.946	0.035	0.023	E
OGLE053308.07-701705.0	113390	5:33:08.07	-70:17:05.0	114.9	2450404.6	16.072	17.512	18.894	0.053	0.042	
OGLE053303.01-701651.7	19730	5:33:03.01	-70:16:51.7	73.18	2450418.5	17.078	18.288	20.213	0.039	0.027	
OGLE053506.92-701632.1	290414	5:35:06.92	-70:16:32.1	857.9	2449618.7	14.917	16.738	-	0.049	0.013	E,LMC_SC16
OGLE053348.74-701608.3	206947	5:33:48.74	-70:16:08.3	89.95	2450385.1	16.704	18.064	19.552	0.067	0.067	
OGLE053301.61-701538.5	25473	5:33:01.61	-70:15:38.5	68.17	2450404.2	16.677	17.913	19.109	0.082	0.073	
OGLE053255.66-701312.2	25439	5:32:55.66	-70:13:12.2	195.8	2450320.3	15.993	17.405	18.828	0.017	0.012	
OGLE053406.23-701149.8	212174	5:34:06.23	-70:11:49.8	102.1	2450419.3	16.300	17.773	19.173	0.039	0.033	
OGLE053233.48-701021.7	31634	5:32:33.48	-70:10:21.7	96.36	2450430.6	16.121	17.462	18.796	0.078	0.068	LMC_SC2
OGLE053318.71-700941.6	124851	5:33:18.71	-70:09:41.6	179.3	2450323.8	16.406	17.769	19.166	0.032	0.027	
OGLE053355.08-700823.8	217550	5:33:55.08	-70:08:23.8	163.6	2450381.0	16.483	17.995	19.418	0.023	0.020	
OGLE053510.14-700755.0	301214	5:35:10.14	-70:07:55.0	496.7	2450113.0	14.886	-	-	0.031	0.021	LMC_SC16
OGLE053327.14-700751.6	130673	5:33:27.14	-70:07:51.6	343.2	2450175.0	15.239	16.835	18.339	0.039	0.028	E
OGLE053415.75-700718.7	217491	5:34:15.75	-70:07:18.7	234.5	2450255.8	15.115	16.985	18.729	0.170	0.121	
OGLE053423.77-700706.8	217589	5:34:23.77	-70:07:06.8	80.20	2450373.2	16.759	17.971	19.083	0.067	0.053	
OGLE053226.48-700604.7	44635	5:32:26.48	-70:06:04.7	454.1	2450428.2	15.047	16.898	18.688	0.068	0.052	E,LMC_SC2
OGLE053422.56-700546.6	223126	5:34:22.56	-70:05:46.6	290.6	2450286.1	15.603	17.352	19.106	0.029	0.023	E
OGLE053357.47-700529.1	223087	5:33:57.47	-70:05:29.1	395.1	2450150.8	14.798	16.771	18.687	0.097	0.064	
OGLE053238.26-700433.6	44721	5:32:38.26	-70:04:33.6	165.9	2450393.4	15.348	16.733	18.110	0.026	0.018	LMC_SC2
OGLE053233.26-700433.5	44720	5:32:33.26	-70:04:33.5	229.4	2450293.9	15.600	17.194	18.721	0.038	0.032	LMC_SC2
OGLE053419.00-700421.3	223158	5:34:19.00	-70:04:21.3	135.7	2450439.0	16.027	17.664	19.315	0.063	0.042	
OGLE053324.13-700241.2	137222	5:33:24.13	-70:02:41.2	23.48	2450430.7	16.924	17.542	17.823	0.070	0.051	
OGLE053504.54-700239.1	307018	5:35:04.54	-70:02:39.1	47.22	2450408.0	16.744	18.019	18.990	0.070	0.043	LMC_SC16
OGLE053456.76-700217.0	312758	5:34:56.76	-70:02:17.0	261.1	2450219.9	15.066	17.133	-	0.097	0.076	LMC_SC16
OGLE053420.26-700213.8	229502	5:34:20.26	-70:02:13.8	404.2	2450082.3	15.530	16.856	17.855	0.022	0.019	
OGLE053433.25-700132.0	312798	5:34:33.25	-70:01:32.0	128.4	2450402.7	15.924	17.406	18.714	0.028	0.021	
OGLE053358.34-700054.4	229486	5:33:58.34	-70:00:54.4	310.5	2450222.7	15.109	16.803	18.798	0.094	0.075	
OGLE053444.35-700031.4	312922	5:34:44.35	-70:00:31.4	122.8	2450356.3	16.419	17.788	19.169	0.026	0.021	
OGLE053258.12-700020.5	51937	5:32:58.12	-70:00:20.5	110.6	2450448.5	16.435	17.826	-	0.071	0.067	
OGLE053422.95-695814.1	235827	5:34:22.95	-69:58:14.1	468.0	2450436.3	15.371	16.902	18.527	0.038	0.031	
OGLE053459.27-695755.1	318682	5:34:59.27	-69:57:55.1	78.74	2450428.3	15.408	16.686	17.740	0.168	0.091	LMC_SC16
OGLE053319.66-695714.6	150929	5:33:19.66	-69:57:14.6	220.1	2450323.3	14.776	15.868	16.560	0.033	0.026	
OGLE053241.26-695648.0	59891	5:32:41.26	-69:56:48.0	15.67	2450435.2	17.730	18.878	19.872	0.130	0.112	
OGLE053358.19-695643.6	235791	5:33:58.19	-69:56:43.6	204.6	2450430.5	15.029	16.601	18.081	0.117	0.113	
OGLE053305.72-695639.8	59340	5:33:05.72	-69:56:39.8	481.6	2450266.0	15.522	17.143	18.816	0.038	0.033	
OGLE053413.75-695636.1	235794	5:34:13.75	-69:56:36.1	311.7	2450140.9	14.842	16.541	18.541	0.025	0.018	
OGLE053248.55-695634.6	59343	5:32:48.55	-69:56:34.6	391.6	2450367.2	15.564	17.043	18.404	0.018	0.015	
OGLE053438.78-695634.1	318659	5:34:38.78	-69:56:34.1	384.7	2450296.1	14.699	16.692	18.415	0.049	0.045	
OGLE053305.21-695623.7	59348	5:33:05.21	-69:56:23.7	125.8	2450370.2	16.179	17.629	18.947	0.047	0.039	
OGLE053351.92-695604.8	235799	5:33:51.92	-69:56:04.8	233.5	2450432.1	14.981	16.197	17.370	0.018	0.005	
OGLE053302.11-695537.8	59366	5:33:02.11	-69:55:37.8	208.2	2450332.4	15.500	17.292	18.891	0.052	0.040	
OGLE053245.16-695524.7	66515	5:32:45.16	-69:55:24.7	67.61	2450404.2	15.905	17.236	18.493	0.118	0.067	
OGLE053418.79-695523.1	242700	5:34:18.79	-69:55:23.1	53.25	2450406.6	16.615	17.858	19.609	0.095	0.083	
OGLE053500.93-695355.2	325028	5:35:00.93	-69:53:55.2	216.1	2450360.0	15.295	16.988	18.633	0.123	0.091	LMC_SC16
OGLE053409.59-695311.0	242787	5:34:09.59	-69:53:11.0	39.41	2450426.7	16.602	17.764	18.799	0.139	0.110	
OGLE053309.47-695238.1	158043	5:33:09.47	-69:52:38.1	229.1	2450224.0	15.390	16.823	18.267	0.045	0.016	
OGLE053309.75-694957.5	164389	5:33:09.75	-69:49:57.5	232.7	2450252.5	15.685	17.237	18.802	0.030	0.025	
OGLE053304.04-694908.9	73016	5:33:04.04	-69:49:08.9	371.0	2450353.5	15.209	16.985	18.644	0.047	0.023	

Remarks: U – uncertain, E – eccentric orbit, LMC_SC? – the same stars in the field LMC_SC?

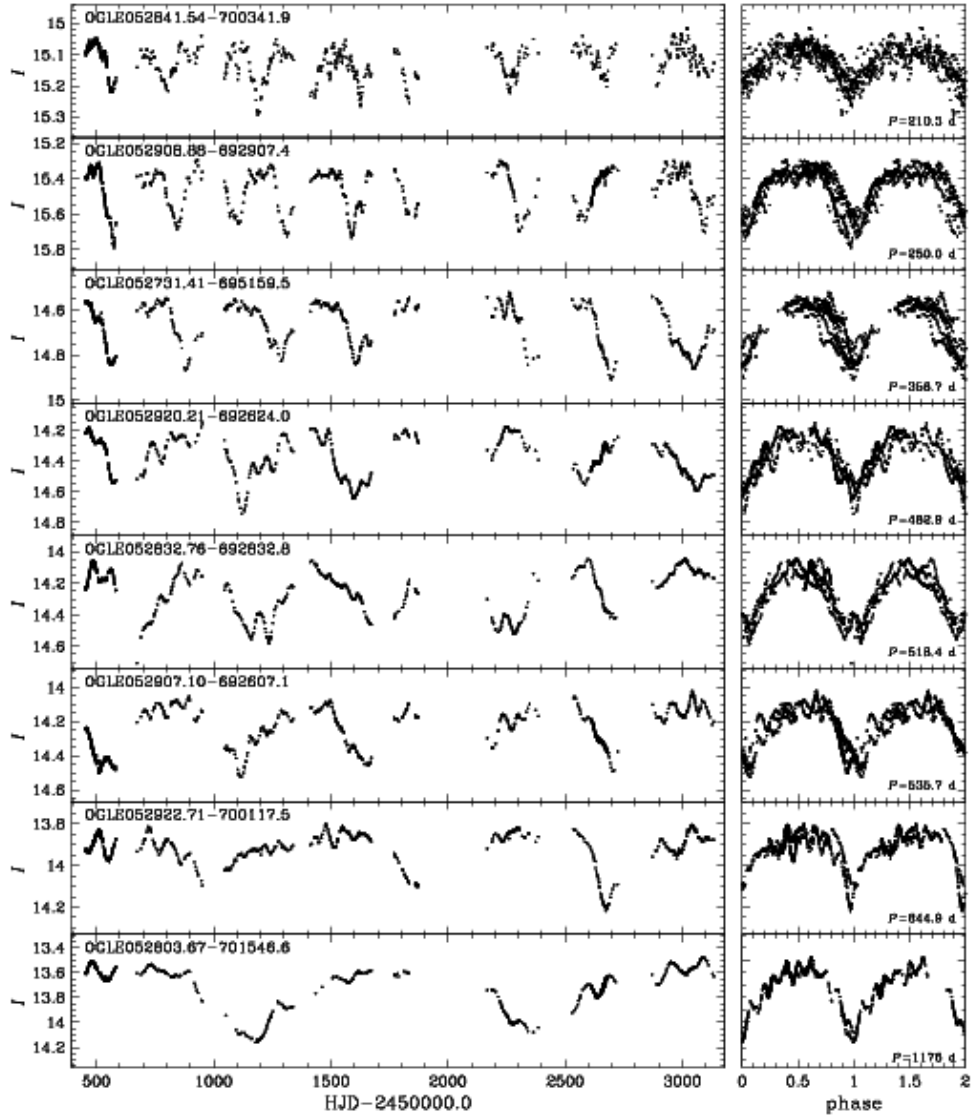


Fig. 4. Light curves of the exemplary LSP red giants in the LMC.

indicate our candidates for the ellipsoidal variables. It is worth noticing that apart from the $P-L$ sequence D presented for the first time by Wood *et al.* (1999), Fig. 5 reveals additional sequence (marked by D') of stars with longer periods.

It is not surprising that the ellipsoidal variability leads to a rather narrow band in the $\log P-W_I$ diagram. Along the red giant branch stellar radius, R

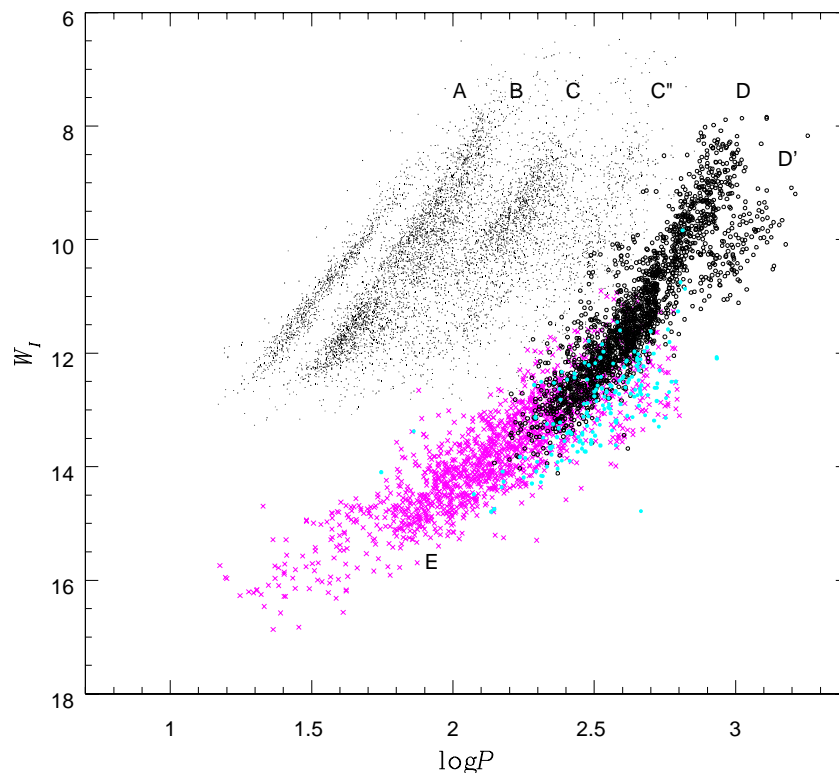


Fig. 5. Period– W_I diagram for variable red giants in the LMC. Magenta crosses mark candidates for ellipsoidal variables, cyan dots show ellipsoidal variables with eccentric orbits, empty circles indicate LSPs, and small dots show other red giants.

increases by more than two orders of magnitude. The luminosity increase is dominated by the radius increase and the period, which cannot be much longer than P_{orb} given in Eq. (1), is determined primarily by the value of $R^{1.5}$.

The striking feature clearly seen in Fig. 5 is that the sequence of ellipsoidal variables partly overlaps with the sequence D and is a continuation of this sequence toward fainter stars. It might suggest binary origin of the LSP phenomenon in the red giants.

Moreover, there is no doubt that some of the LSP cases may be explained by ellipsoidal variability. Fig. 6 presents exemplary light curves of stars where the characteristic OSARG variability is superimposed on the evident ellipsoidal light curves. We found about 300 such objects, mostly among brighter stars. The shorter, small amplitude variability corresponds to OSARG’s period–luminosity sequences (Soszyński *et al.* 2004).

However, there are several serious differences between ellipsoidal variables and typical LSP giants. First, typical LSP light curve is not double humped, like the ellipsoidal light modulation (*cf.* Fig. 1 and Fig. 4). Second, the typical period – amplitude relation for the LSP variables is different than for the ellipsoidal

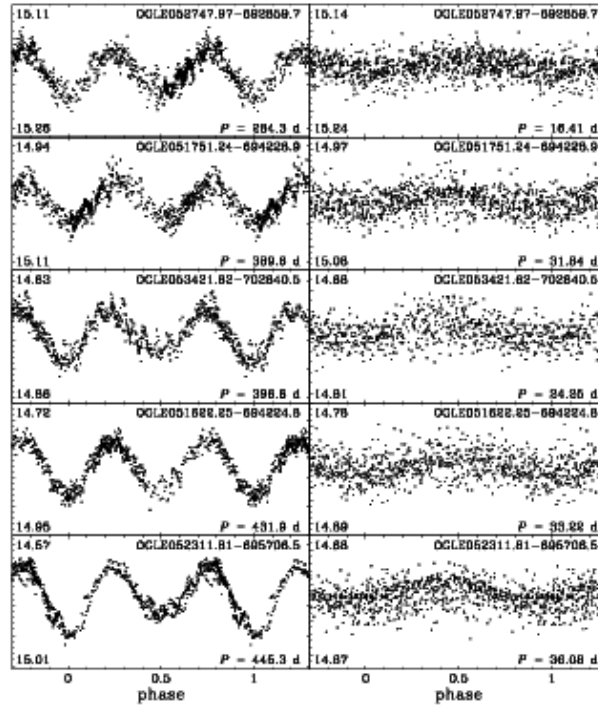


Fig. 6. Light curves of the ellipsoidal candidates exhibiting simultaneously OSARG-type variability. *Left column* shows folded ellipsoidal light curves, and *right column* presents OSARG light curves after subtracting the dominant variability.

giants. The amplitudes of LSP variability are positively correlated with the brightness of the star, while in ellipsoidal variables the amplitudes are connected only with the dispersion of the PL relation (Fig. 3). Third, Wood, Olivier and Kawaler (2004) noticed that the binary origin of the LSP is difficult to accept on statistical ground. LSP occurs in one third of the AGB stars, while the ellipsoidal variability relates to less than 1% of the analysed giants.

The $\log P - W_I$ correlation for the LSP is very significant and cannot be ignored in any explanation of phenomenon. If the stars are forced to rotate at nearly break up velocity, then we expect a $P_{\text{rot}}(\bar{\rho})$ relation, the same as that given in Eq. (1), but with $f = 1.2$. Any asymmetry about the rotation axis could produce light variation with the P_{rot} . However, the implied equatorial velocities of rotation seems unacceptably large. For instance at $\log P \approx 2.5$ we obtain the value of about 30 km/s.

The explanation favored by Wood, Olivier and Kawaler (2004) (an excitation of a g-mode trapped above the convective envelope) may also explain the observed correlation. However, properties of such modes and chances of their driving remain to be studied.

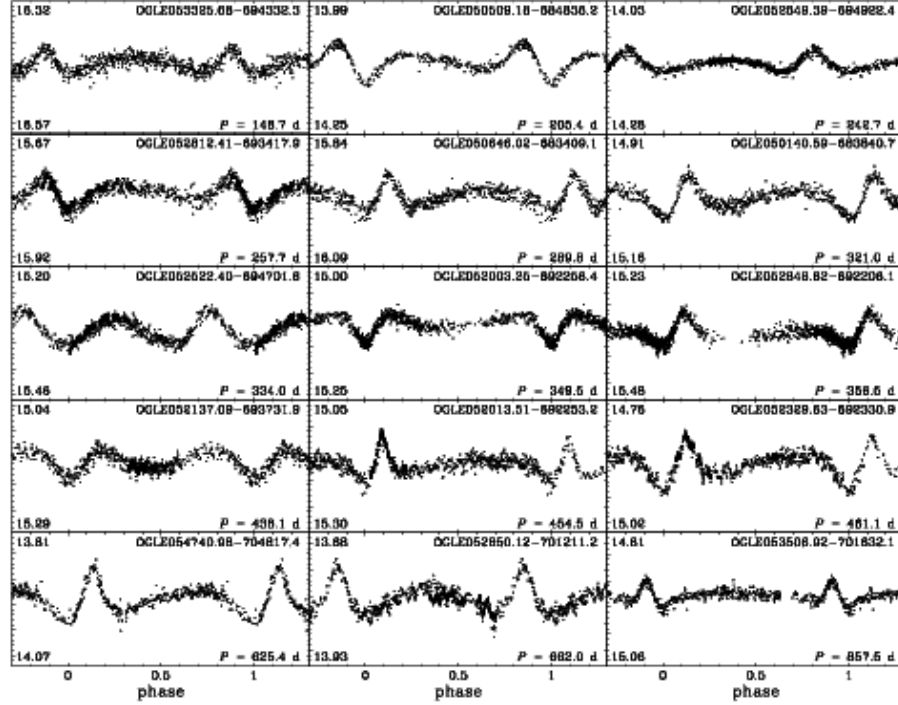


Fig. 7. Light curves of the exemplary ellipsoidal red giants with eccentric orbits.

6. Ellipsoidal Systems with Eccentric Orbits

About 10% of candidates for ellipsoidal variables show evident deviations from symmetric sinusoidal light curves. For a sample of 165 objects the shapes of the light curves are completely different than typical sine-wave light curves of the ellipsoidal variables. Examples of these light curves are presented in Fig. 7. One should notice a large variety of the light curves.

An explanation of such variables was proposed by B. Paczyński (2004, private communication) who suggested that these objects may be ellipsoidal systems with significant eccentricity of the orbits. A similar periodic light curve, although with the period of about 4 days, is shown by the well-studied star α Vir (Spica). Photometric and spectroscopic measurements showed that it is an ellipsoidal binary system with significant eccentricity of the orbit, equal to 0.14. Variable distance of the binary components changes tidal interaction of stars during the orbital movement, which affects the shape of the ellipsoidal modulation. Moreover, the α Vir light curve is changing in the time scale of several dozen years (*cf.* the light curves obtained by Shobbrook *et al.* 1969 and Sterken, Jerzykiewicz and Manfroid 1986), what is an effect of apsidal line rotation. Large variety of the light curves observed in the LMC can be explained by different longitude of the line of apsides.

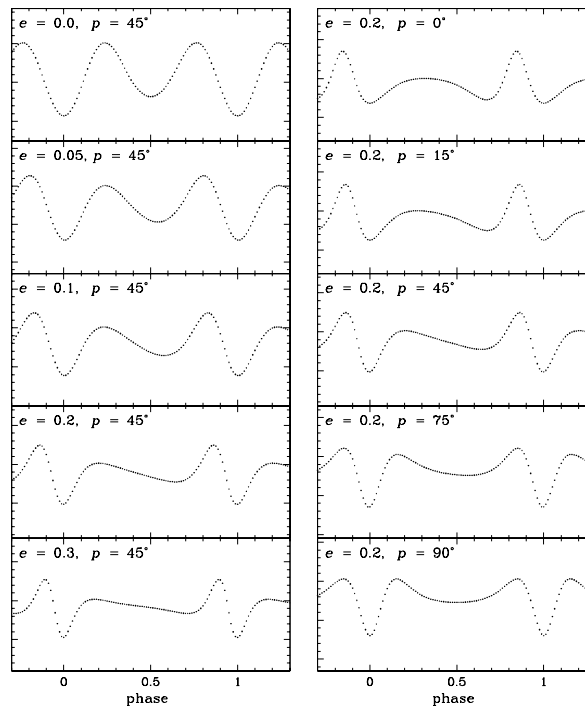


Fig. 8. Model light curves of the ellipsoidal red giants with eccentric orbits. In the *left column* light curves with increasing eccentricity (e) are showed, the *right column* presents a series of light curves produced by binary systems with the eccentricity $e=0.2$, and a different periastron length (p).

To make sure that the variables are binary systems with eccentric orbits, we modeled such light curves using program NIGHTFALL[†] by R. Wichmann. A series of models are presented in Fig. 8. We modeled an equal-mass binary system with one of the components entirely filling the Roche lobe. The inclination angle is equal to 60° . In the left column the light curves with increasing eccentricity (e) are showed, while in the right column we present light curves produced by binaries with the same eccentricity ($e=0.2$), but with a different periastron length (p). One can note clear similarity of the observed and calculated light curves.

The models confirm that the larger eccentricity of the orbit, the more asymmetric light curve is. The variable showing one of the most asymmetric light curve – OGLE052013.51–692253.2 – corresponds to a model with $e=0.4$. However, precise modeling of the binary systems will be possible after obtaining the radial velocity curves.

Verbunt and Phinney (1995) estimated that the circularization time scale of the semi-detached binaries containing a giant is of the order of several thousand

[†] <http://www.lsw.uni-heidelberg.de/users/rwichman/Nightfall.html>

years. This estimation is almost independent of the mass of the companions. Thus, it is very unlikely that the close binaries maintained their initial eccentricity. It is more probable that the eccentricity of the orbits was induced by the rapid mass transfer or interaction of the third companion.

Mechanisms of the orbit circularization induced by the tidal effects were studied by Zahn (1977, 1989) and Tassoul and Tassoul (1992). Such processes are especially effective for the red giants, due to the turbulent viscosity associated to the convective envelopes. Studies of the spectroscopic binary systems containing red giants showed that there exist limiting period below which circularization takes place. Mayor and Mermilliod (1984) analyzed the orbital parameters of 17 spectroscopic binaries with a red giant, and found that orbits are circularized at periods $P < 150$ days, however there are many exceptions to this rule.

Obviously, the circularization time scale depends not only on the semi-major axis of the orbit (and consequently orbital period), but also on the radius of the giant star (related to the luminosity of the object). One can notice this effect in Fig. 5, where the period–luminosity relation of the candidates for eccentric ellipsoidal variables is marked by cyan dots. The magnitudes of objects are clearly correlated with the periods: the brighter stars, the longer orbital period of the system. Moreover, eccentric ellipsoidal variables have typically longer periods than non-eccentric ellipsoidal systems.

7. Summary

In this paper we showed that the ellipsoidal red giants constitute a numerous and homogeneous sample. This class of variables is difficult to detect because of their small amplitudes and long periods. Only long-term observing surveys, obtaining good quality photometry, can trace this type of variability.

Ellipsoidal variables form the PL sequence what is a projection of the radius–luminosity relationship for the red giants. We noticed that PL sequence of the ellipsoidal red giants is a continuation of the sequence of LSP variables, what may suggest a connection of the LSP and the binarity. Some ellipsoidal variables of the longer periods exhibit small-amplitude variability, corresponding to OSARGs.

About 10% of the ellipsoidal variables show characteristic asymmetric light curves, probably caused by close binary systems with eccentric orbits. This sample may become an important test of tidal circularization theories.

Acknowledgements. We would like to thank Prof. Bohdan Paczyński, whose suggestions enabled us to explain the mystery of ellipsoidal variables with eccentric orbits. The paper was partly supported by the Polish KBN grant 2P03D02124 to A. Udalski. Partial support to the OGLE project was provided with the NSF grant AST-0204908 and NASA grant NAG5-12212 to B. Paczyński.

REFERENCES

- Alard, C., and Lupton, R.H. 1998, *Astrophys. J.*, **503**, 325.
- Alard, C. 2000, *Astron. Astrophys. Suppl. Ser.*, **144**, 363.
- Davidge, T.J., and Milone, E.F. 1984, *Astrophys. J. Suppl. Ser.*, **55**, 571.
- Girardi, L., Bertelli, G., Bressan, A., Chiosi, C., Groenewegen, M.A.T., Marigo, P., Salasnich, B., and Weiss, A. 2002, *Astron. Astrophys.*, **391**, 195.
- Hall, D. 1990, *Astron. J.*, **100**, 554.
- Kurucz, R.L. 1998, <http://cfaku5.cfa.harvard.edu>.
- Mayor, M. and Mermilliod, J.-C. 1984, *IAU Symp.*, 105, "Observational Tests of the Stellar Evolution Theory", Eds. A. Maeder and A. Renzini Reidel (Dordrech), p. 411.
- Morris, S. 1985, *Astrophys. J.*, **295**, 143.
- Paczyński, B. 1971, *Ann. Rev. Astron. Astrophys.*, **9**, 183.
- Schechter, P.L., Mateo, M., and Saha, A. 1993, *P.A.S.P.*, **105**, 1342.
- Shobbrook, R.R., Herbison-Evans, D., Johnston, I.D., and Lomb, N.R. 1969, *MNRAS*, **145**, 131.
- Soszyński, I., Udalski, A., Kubiak, M., Szymański, M., Pietrzyński, G., Żebruń, K., Szewczyk, O., and Wyrzykowski, L. 2004, *Acta Astron.*, **54**, 129.
- Sterken, C., Jerzykiewicz, M., and Manfroid, J. 1986, *Astron. Astrophys.*, **169**, 166.
- Tassoul, J.-L., and Tassoul M. 1992, *Astrophys. J.*, **395**, 259.
- Udalski, A. 2003, *Acta Astron.*, **53**, 291.
- Udalski, A., Kubiak, M., and Szymański, M. 1997, *Acta Astron.*, **47**, 319.
- Udalski, A., Szymański, M., Kubiak, M., Pietrzyński, G., Soszyński, I., Woźniak, P.R., and Żebruń, K. 2000, *Acta Astron.*, **50**, 307.
- Verbunt, F., and Phinney, E.S. 1995, *Astron. Astrophys.*, **296**, 709.
- Wood, P.R., *et al.* 1999, in *IAU Symp.*, 191, "Asymptotic Giant Branch Stars", Ed. T. Le Bertre, A. Lébre, and C. Waelkens (San Francisco: ASP), 151.
- Wood, P.R., Olivier, E.A., and Kawaler, S.D. 2004, *Astrophys. J.*, **604**, 800.
- Woźniak, P.R. 2000, *Acta Astron.*, **50**, 421.
- Wray, J.J., Eyer, L., and Paczyński, B. 2004, *MNRAS*, **349**, 1059.
- Wyrzykowski, L., Udalski, A., Kubiak, M., Szymański, M., Żebruń, K., Soszyński, I., Woźniak, P.R., Pietrzyński, G., and Szewczyk, O. 2003, *Acta Astron.*, **53**, 1.
- Zahn, J.-P. 1977, *Astron. Astrophys.*, **57**, 383.
- Zahn, J.-P. 1989, *Astron. Astrophys.*, **220**, 112.